INSTITUT DE FRANCE
Académie des sciences

Comptes Rendus
Mécanique

Said Mesmoudi, Omar Askour and Bouazza Braikat

Radial point interpolation method and high-order continuation for solving nonlinear transient heat conduction problems

Volume 348, issue 8-9 (2020), p. 745-758

Published online: 14 December 2020

https://doi.org/10.5802/crmeca.49

Les Comptes Rendus. Mécanique *sont membres du Centre Mersenne pour l'édition scientifique ouverte*
www.centre-mersenne.org
e-ISSN : 1873-7234

Comptes Rendus
Mécanique
2020, 348, nº 8-9, p. 745-758
https://doi.org/10.5802/crmeca.49

Historical article / *Article historique*

Radial point interpolation method and high-order continuation for solving nonlinear transient heat conduction problems

Said Mesmoudi [a], **Omar Askour** [a] **and Bouazza Braikat** [*, a]

[a] Laboratoire d'Ingénierie et Matériaux, Faculté des Sciences Ben M'sik, Hassan II University of Casablanca, Avenue Driss El Harti, B.P. 7955 Sidi Othman, Casablanca, Morocco

E-mails: mesmoudisaiid@gmail.com (S. Mesmoudi), o.askour1@gmail.com (O. Askour), b.braikat@gmail.com (B. Braikat)

Abstract. In this work, we propose the investigation of unsteady nonlinear heat conduction by using the radial point interpolation method (RPIM) in high-order continuation coupled with homotopy transformation for the first time. In this resolution strategy, the Euler implicit time scheme is used to transform the unsteady nonlinear continuous problem into a sequence of stationary continuous problems. Moreover, by using the RPIM, we transform the sequence of stationary nonlinear continuous problems into discrete problems. Then, homotopy transformation is applied by introducing an arbitrary invertible pre-conditioner $[K^*]$ and a dimensionless parameter a. These nonlinear problems are transformed into a sequence of linear problems thanks to Taylor series expansions used in a continuation technique to compute the whole solution branch by branch. Numerical examples have been investigated to show the accuracy and efficiency of the proposed approach in this type of problem. The results obtained by the proposed high-order homotopic continuation with the RPIM are compared with those computed by the Newton–Raphson method coupled with the RPIM, high-order homotopic continuation with moving least squares, and high-order homotopic continuation with the finite element method.

Keywords. Radial point interpolation method (RPIM), Homotopy transformation, High-order continuation, Heat conduction, Thermal conductivity.

Manuscript received 11th May 2020, revised 25th July 2020, accepted 15th September 2020.

1. Introduction

The determination of temperature and its distribution inside heat conducting materials depends on the boundary conditions imposed to control the operating states of these materials. Therefore, it is necessary to control this thermal variable in these conducting materials. The prediction of temperature-dependent material properties requires the resolution of nonlinear transient heat conduction problems. For example, thermal conductivity is assumed to be a function of

* Corresponding author.

temperature when its gradient is significantly large [1–7]. To that effect, several numerical resolution methods based on the finite element method (FEM), the finite volume method, the finite difference method (FDM), and so on have been developed for analysing this type of problem. However, the re-meshing used by these methods and the complex geometry of the structures require considerable computation time; sometimes, in these conditions, these methods diverge. For this reason, several other numerical methods, the so-called mesh-free methods, have been developed during the past decades. These methods, such as the reference methods, permit us to overcome difficulties with regard to re-meshing and complex geometries [8–14]. The principle of these methods is based on a set of arbitrarily scattered nodes in the studied domain to approximate unknown solutions without the notion of connectivity [8]. According to the type of weak formulation, there are two general classes of meshless methods. The first class is based on a global weak formulation such as the element-free Galerkin (EFG) method [7], while the second class is based on a local weak formulation in which the meshless local Petrov–Galerkin method is the most popular [11, 13]. In addition, we distinguish two classes of meshless methods such as the approximation methods and the interpolation methods. The first class is based on moving least squares (MLS) approximants to construct the shape function [8, 11, 12]. The second class deals with interpolation methods, where shape functions have the Kronecker delta function property, such as the point interpolation method (PIM) and the radial point interpolation method (RPIM) [9, 10, 14, 15].

Based on the FEM, many applications of high-order continuation (HOC) coupled with homotopy transformation show the performance of this technique with respect to computation time, automatic adaptability of the step length, and the exactness of solutions in structural and fluid mechanics [16–19]. In addition, the meshless method such as MLS approximation is coupled with HOC for the resolution of dynamic or static nonlinear problems [20–28]. Meshless methods such as MLS approximation have some difficulties in the treatment of essential boundary conditions. Indeed, the use of MLS approximation in two or three dimensions does not give an exact interpolation of unknowns on the boundary even if collocation methods are used. Other meshless methods, such as the RPIM [10, 14, 15] permit to check exactly the boundary conditions. This method makes the imposition of boundary conditions much easier than the other meshless methods.

In this work, we propose the investigation of unsteady nonlinear heat conduction by using the RPIM in HOC coupled with homotopy transformation for the first time. This approach consists in coupling a temporal implicit Euler scheme and homotopy transformation with the HOC developed in [29]. To demonstrate the efficiency and accuracy of this algorithm, two examples are discussed. In the first example, we compare the results obtained by the proposed approach, high-order homotopic continuation with the radial point interpolation method (HOHC-RPIM), with those calculated by the Newton–Raphson method [30, 31]. It should be noted that the Newton–Raphson method is coupled with the RPIM for the first time. In the second example, a comparison is made among the results obtained by three approaches, HOHC-RPIM, high-order homotopic continuation with moving least squares (HOHC-MLS), and high-order homotopic continuation with the finite element method (HOHC-FEM).

This paper is organized as follows. The mathematical formulation of heat conduction problems with temperature-dependent conductivity is described in Section 2. A short description of RPIM shape functions is presented in Section 3. Section 4 is devoted to the resolution strategy of the considered problem by the HOHC-RPIM algorithm. Some discussions of the efficiency and the ability of the proposed approach in numerical examples are presented in Section 5. A conclusion on the analysis of the obtained results is given in Section 6 followed by a bibliography list.

2. Mathematical formulation of unsteady nonlinear heat conduction problem with temperature-dependent conductivity

We consider a thermally isotropic bidimensional domain Ω. When the generated and viscous dissipation are neglected, the transient heat conduction problem is governed by

$$\rho C_p \frac{\partial T(X,t)}{\partial t} = \frac{\partial}{\partial x}\left(k(T)\frac{\partial T(X,t)}{\partial x}\right) + \frac{\partial}{\partial y}\left(k(T)\frac{\partial T(X,t)}{\partial y}\right) \quad \text{in } \Omega \quad \text{for } t \geq 0, \tag{1}$$

where $T(X,t)$ is the temperature on the domain Ω surrounded by closed boundaries Ω_D and Ω_N, t is a temporal variable, and X denotes the physical dimensions expressed in Cartesian coordinates, $X = (x,y)$. The parameters ρ, C_p, and $k(T)$ are respectively mass density, specific heat capacity, and thermal conductivity of the solid occupying the domain Ω. It should be noted that the mass density and the specific heat capacity are considered as constants in this study. However, the thermal conductivity depends nonlinearly on the temperature as presented in some works [4, 5, 32–34]. The above equation is completed by the initial and boundary conditions as follows:

$$\begin{cases} T(X,t) = T^0(X) \text{ in } \Omega & \text{for } t = 0, \\ T(X,t) = T^d(X) \text{ over } \Omega_D & \text{for } t \geq 0, \\ -k(T)\dfrac{\partial T(X,t)}{\partial N} = q^d(X,t) \text{ over } \Omega_N & \text{for } t \geq 0, \end{cases} \tag{2}$$

where N is the unit outward normal vector to the boundary Ω_N, $T^0(X)$ is the initial condition, $T^d(X)$ is the imposed temperature on the boundary Ω_D, and $q^d(X,t)$ is the applied heat flux through the boundary Ω_N. The strong nonlinearity treated in this work regards the conductivity, which is expressed at point X as $k(T) = k_0 + eT^2(X,t)$, where k_0 and e are given constants. Different expressions of $k(T)$ are considered by several works [1, 3–6].

Based on the meshless methods in weak form, the nonlinear problem (1) has been usually solved by several authors in the literature. Indeed, in [4, 5, 34], the authors have used a radial integration boundary element method to solve nonlinear heat conduction with temperature-dependent thermal conductivity in stationary and transient cases. Juan *et al.* [7] have proposed an alternative resolution for the heat transfer problem involved in direct-chill casting processes employing the EFG method. A dual-reciprocity boundary element method was used also in [30]. This numerical method was proposed to solve a unsteady axisymmetric heat conduction problem involving a non-homogeneous solid with temperature-dependent properties. On the other hand, meshless methods in strong form have been employed also for solving this problem using iterative solvers such as in [6, 35]. Our contribution in this work regards the use of RPIM in high-order homotopic continuation in strong form for solving this problem. It is preferable to start by a short description of the RPIM shape function.

3. Description of radial point interpolation method

The RPIM only needs to construct the variable shape function using the nodes that are distributed in the domain [11]. The variable shape function is a series representation of the unknown function evaluated at a node using a set of arbitrarily scattered nodes localized in a local support domain (see Figure 1).

To avoid the dependence between the locations of the nodes in the support domain and the terms of monomials used in the conventional PIM, the radial basis function (RBF) is used to construct the RPIM [10, 11, 15]. The coupling of the PIM with the RBF permits us to impose correctly the boundary conditions. The approximation of the unknown $T(X,t)$ at a node of

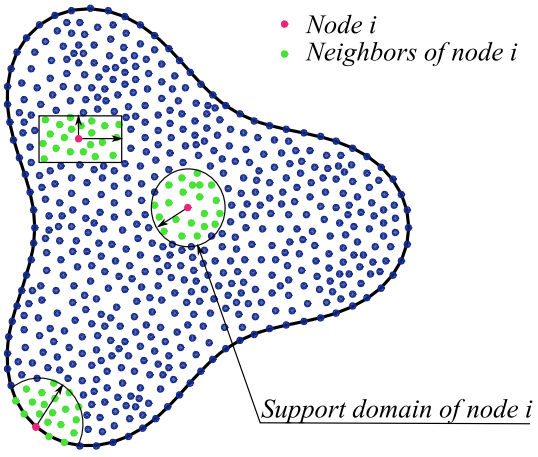

Figure 1. Local support domains for an arbitrary node i in a two-dimensional hypothesis domain.

interest of coordinate X using its neighbours $\bar{X}$ by the RPIM for fixed time t is defined in the following form:

$$\begin{aligned} T(X,t) &= \sum_{i=1}^{i=n_s} R_i(X)\alpha_i + \sum_{j=1}^{j=m} p_j(X)\beta_j \\ &= \langle R(X), P(X)\rangle \begin{Bmatrix} \alpha \\ \beta \end{Bmatrix}, \end{aligned} \tag{3}$$

where $\langle R(X)\rangle = \langle R_1(X), R_2(X), \ldots, R_{n_s}(X)\rangle$ is the RBF, $\langle P(X)\rangle = \langle p_1(X), p_2(X), \ldots, p_m(X)\rangle$ is a monomial in space coordinates, n_s is the number of RBFs, m is the number of polynomial basis functions, and coefficients ${}^t\{\alpha\} = \langle \alpha_1, \alpha_2, \ldots, \alpha_{n_s}\rangle$ and ${}^t\{\beta\} = \langle \beta_1, \beta_2, \ldots, \beta_m\rangle$ are new unknowns yet to be determined. However, there are $n_s + m$ variables in (3). It is necessary to add the following m constraint conditions:

$$\sum_{i=1}^{n_s} p_j(\bar{X}_i)\alpha_i = 0 \quad \text{for } j = 1, 2, \ldots, m. \tag{4}$$

In (3), the terms $R_i(X)$ are calculated from the Euclidean distance $r_i = \|X - \bar{X}_i\|$ between the node of interest X and its neighbours $\bar{X}_i$ as follows:

$$\begin{cases} R_i(X) = (r_i^2 + c^2)^q & \text{multiquadrics } (MQ), \\ R_i(X) = r_i^l \ln(r_i) & \text{thin plate spline } (TPS), \\ R_i(X) = e^{-(qr_i)^2} & \text{Gaussian } (EXP), \end{cases} \tag{5}$$

where MQ, TPS, and EXP are types of RBFs that can be used for calculating the terms $R_i(X)$ [36–38]. The parameters c, q, and l can be selected from the numerical tests of each function to stabilize the solution or by using algorithms designed for their determination. In the present work, the selected values of these parameters are chosen from numerical tests as in [29]. The term $p_j(X)$ in (3) is formulated using Pascal's triangle, and a complete basis is usually preferred with $m = 3$, $m = 6$, or $m = 10$ for the linear, the quadratic or the cubic basis function, respectively. The details of the RPIM shape function's construction from (3) are given in [29].

4. Resolution strategy

Recall that to solve nonlinear heat conduction with temperature-dependent thermal conductivity (1), we propose high-order mesh-free homotopic continuation. This approach combines a temporal implicit Euler scheme, the RPIM method, the homotopy transformation, a Taylor series expansion, and a continuation procedure.

4.1. *Temporal implicit Euler scheme*

In this section, for solving the nonlinear unsteady problem (1), we apply the temporal implicit Euler scheme widely used in the resolution of transient problems [21,23,27] as

$$\rho C_p \frac{T^{n+1}-T^n}{\Delta t} = G_1(k^{n+1}, T^{n+1}) \quad \text{for } t^{n+1} = (n+1)\Delta t, \tag{6}$$

where $G_1(\bullet,\bullet) = \partial/\partial x(\bullet\partial\bullet/\partial x) + \partial/\partial y(\bullet\partial\bullet/\partial y)$. By evaluating the unknown between the current time step and the next time step, we introduce new unknowns $\Delta T = T^{n+1} - T^n$ and $\Delta k = k^{n+1} - k^n$ in the above equation as follows:

$$\begin{cases} L(\Delta T) + Q(\Delta k, \Delta T) = F^n & \text{in } \Omega, \\ \Delta k = 2eT^n\Delta T + e\Delta T^2 & \text{in } \Omega, \\ \Delta T = 0 & \text{over } \Omega_D, \\ k^n \dfrac{\partial \Delta T}{\partial N} + \Delta k \dfrac{\partial T^n}{\partial N} = -\Delta k \dfrac{\partial \Delta T}{\partial N} & \text{over } \Omega_N, \end{cases} \tag{7}$$

where $L(\Delta T) = \rho C_p \Delta T - \Delta t G_1(k^n, \Delta T) - \Delta t G_1(\Delta k, T^n)$ and $Q(\Delta k, \Delta T) = -\Delta t G_1(\Delta k, \Delta T)$ are respectively the linear and quadratic operators and $F^n = \Delta t G_1(k^n, T^n)$ is a known second member evaluated at $t^n = n\Delta t$.

4.2. *High-order continuation with homotopy transformation*

In the second method, the RPIM approximation of the new principal unknown ΔT is used. Therefore, by using the shape functions defined in [29], this unknown is approximated at a node of coordinate X as follows:

$$\Delta T(X) = \langle \Phi(X) \rangle \{\Delta T_s\}, \tag{8}$$

where $\langle \Phi(X) \rangle$ is the vector of shape functions corresponding to n_s nodes in the support domain of the node X and $\{\Delta T_s\}$ is the vector that collects the nodal unknowns for all nodes in the support domain. Taking into account (8) and following an assembly technique, problem (7) verified by a new unknown can be written as

$$\begin{cases} [K_T^n]\{\Delta T\} + \{Q(\Delta T, \Delta T)\} = \{F^n\}, \\ \Delta k(X) = e(2T^n)(X)\langle \Phi(X) \rangle \{\Delta T_s\} + \langle \Delta T_s \rangle \{\Phi(X)\} \langle \Phi(X) \rangle \{\Delta T_s\}, \end{cases} \tag{9}$$

where $[K_T^n]$ is the tangent matrix that depends on the solution at time t^n, $\{\Delta T\}$ is the global vector containing N_p components with N_p being the total number of nodes in the domain Ω, $\{Q(\Delta T, \Delta T)\}$ is a vectorial nonlinear quadratic form, and $\{F^n\}$ is the second member that depends on the solution at time t^n.

To avoid the decomposition of the tangent matrix at each time step by the iterative solvers as presented in [4,5], we use homotopy transformation by introducing an arbitrary matrix $[K^*]$ and an artificial parameter a in the following form:

$$[K^*]\{\Delta\theta\} + a([K_T^n] - [K^*])\{\Delta\theta\} + \{Q(\Delta\theta, \Delta\theta)\} = a\{F^n\}, \tag{10}$$

where a is a parameter that permits us to transform problem (9) into problem (10) whose solution $\{\Delta\theta\}$ coincides with that of (9) when $a = 1$. The solution of problem (10) is sought from the Taylor series expansion truncated at order P as follows:

$$\{\Delta\theta(a)\} = a\{\Delta\theta_1\} + a^2\{\Delta\theta_2\} + \cdots + a^P\{\Delta\theta_P\}. \tag{11}$$

By introducing Taylor series (11) in the artificial problem (10) and by regrouping the terms taking into account the power of a, we obtain the following linear problems:

$$\begin{aligned} &\text{Order } i = 1: \quad [K^*]\{\Delta\theta_1\} = \{F^n\}, \\ &\text{Order } 2 \le i \le P: \quad [K^*]\{\Delta\theta_i\} = ([K^*] - [K_T^n])\{\Delta\theta_{i-1}\} + \{F_i^{nl}\}, \end{aligned} \tag{12}$$

where $\{F_i^{nl}\}$ is the second member at order i that depends on the previous orders. Using a continuation procedure, Taylor series (11) has a validity range $[0, a_{\max}]$. The parameter a should be greater than or equal to one for computing solution (11). The validity range $a_{\max}$ is described in [16, 23, 27, 39] as

$$a_{\max}(t) = \left(\kappa \frac{\|\{\Delta\theta_1\}\|}{\|\{\Delta\theta_P\}\|}\right)^{\left(\frac{1}{P-1}\right)}, \tag{13}$$

where κ is a given tolerance and $\|\bullet\|$ is the classical norm L_2. If $a_{\max}(t_{n+1}) \ge 1$, then we can deduce the solution at time $t_{n+1} = (n+1)\Delta t$ of problem (6) in the following form:

$$\{T^{n+1}\} = \{T^n\} + \{\Delta\theta(a = 1)\}. \tag{14}$$

5. Numerical applications and discussion

To illustrate the efficiency and the reliability of the proposed approach, two numerical examples of nonlinear transient heat conduction with different boundary conditions are investigated in this section. Both the examples deal with two-dimensional (2D) heat conduction over a square plate and over a perforated circular plate. The obtained results are presented by a comparison with those results calculated by using the Newton–Raphson method coupled with the radial point interpolation method (NR-RPIM) and with the finite element method (NR-FEM) and also by the same proposed approach using the MLS and FEM approximations. The numerical analysis of the following examples was carried out using a computer with an Intel(R) Core(TM) i3-4160 CPU, 3.60 GHz, with 4 GB of memory.

5.1. *2D heat conduction over a square plate*

In the first example, we consider thermal nonlinear conduction in a square plate of side $L = 1$ m, mass density $\rho = 100$ kg/m^3, and specific heat $C_p = 100$ J/(kg·K) [4, 5, 34, 40]. Dirichlet conditions are imposed on sides AD and BC at $T^d = 100$ and $T^d = 200$ K, respectively, while sides AB and DC are thermally insulated. These boundary conditions are depicted in Figure 2. The initial condition is taken as $T^0 = 100$ K.

The continuous domain occupied by the plate is replaced by 121 nodes. Moreover, the support domain is considered as a circle of radius $h = 2\,\mathrm{d}r$ (see Figure 1), where $\mathrm{d}r$ is the smallest distance between nodes. For the NR-FEM algorithm taken as the reference method, the domain is discretized into 16 599 finite elements of type $T3$. The proposed approach permits us to reduce the number of matrix decompositions used by the iterative solvers. Indeed, the preconditioner matrix $[K^*]$ is taken equal to the tangent matrix $[K_T^n]$ evaluated at the starting time of each continuation step. Then, we retain the same tangent matrix $[K^*]$ for the subsequent time steps if $a(t_n) \ge 1$; if not, then we take the tangent matrix $[K^*] = [K_T^{n\max}]$ for restarting the next continuation step. Here, $n\max$ is the maximal number of time steps at each continuation step.

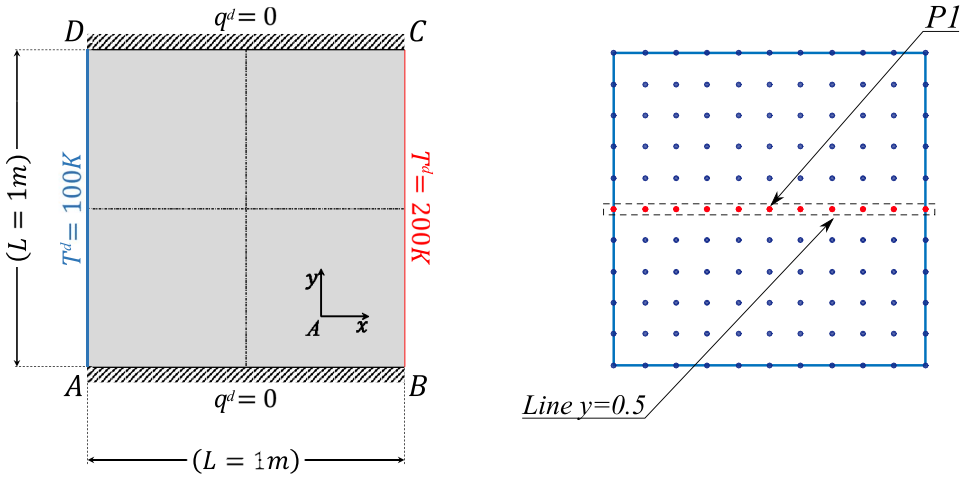

(a) Continuous domain (b) Discrete domain

Figure 2. A square plate under boundary conditions and a discrete domain.

Table 1. Influence of time steps and tolerance parameter on the parameter $a_{\max}(t_n)$ for a truncation order $P = 15$

Tolerance κ	$\Delta t = 1$ s	$\Delta t = 0.1$ s	$\Delta t = 0.01$ s	$\Delta t = 0.001$ s
10^{-1}	$a_{\max}(t_n) < 1$	5.4294	203.6295	5935.9680
10^{-2}	$a_{\max}(t_n) < 1$	3.0531	114.5093	3338.0401
10^{-4}	$a_{\max}(t_n) < 1$	$a_{\max}(t_n) < 1$	36.2110	1055.5809
10^{-6}	$a_{\max}(t_n) < 1$	$a_{\max}(t_n) < 1$	11.4509	333.8040
10^{-8}	$a_{\max}(t_n) < 1$	$a_{\max}(t_n) < 1$	3.6211	105.5580

The parameters and the types of RBFs used in this proposed approach are listed in [29]. Computation is carried out in the time interval $[0, 100s]$ for different time steps so that the influence of each step on the continuation step can be tested. For a truncation order $P = 15$ and for different tolerances, we report in Table 1 the values of the parameter $a_{\max}(t_n)$. From this table, we remark that when the time step decreases for each tolerance parameter, the value of $a_{\max}(t_n)$ increases. From the obtained values of the parameter $a_{\max}(t_n)$, we adopt the time step $\Delta t = 0.1$ s for the following process.

To show the performance and the correctness of the proposed approach HOHC-RPIM, we report in Table 2 the solution quality measured by the Euclidean norm of the residual and the CPU time compared with those of the HOHC-MLS and HOHC-FEM algorithms. In this table, the computation is performed in the interval [0, 30 s], where the temperature reaches the steady state (see Figure 3). From this table, we remark that when the truncation order increases and the tolerance decreases, the solution quality is better, but it is obtained with considerable CPU time. In addition, the approach followed makes it possible to obtain the solution even for a small truncation order $P = 3$ and for a tolerance parameter $\kappa = 10^{-1}$ with an acceptable solution quality and a relatively small computation time compared with the other approaches HOHC-MLS and HOHC-FEM. We also note that for order $P = 3$ and for a tolerance parameter $\kappa = 10^{-1}$, all the algorithms converge but with different solution qualities. Beyond $\kappa = 10^{-1}$, the algorithms diverge because the parameter $a_{\max}$ is lower than 1. From a comparison among the three algorithms, both the algorithms HOHC-RPIM and HOHC-MLS require less computation

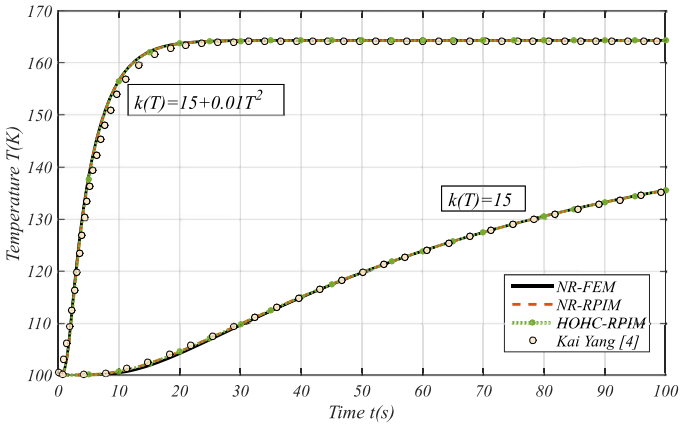

Figure 3. Temporal evolution of temperature at point $P1(0.5, 0.5)$.

Table 2. Numerical results about the effect of algorithm parameters on the solution, the residual norm, and the CPU time for $\Delta t = 0.1$ s

Order	Tolerance	HOHC-FEM		HOHC-MLS		HOHC-RPIM	
		$\log_{10}(\|Re\|)$	CPU (s)	$\log_{10}(\|Re\|)$	CPU (s)	$\log_{10}(\|Re\|)$	CPU (s)
3	10^{-1}	−6.1578	68.4319	−0.5154	1.1297	−4.5596	0.7619
	10^{-2}	$a_{\max}(t_n) < 1$	$a_{\max}(t_n) < 1$	0.9283	1.2260	−0.9015	0.8688
	10^{-4}	$a_{\max}(t_n) < 1$	$a_{\max}(t_n) < 1$	$a_{\max}(t_n) < 1$	$a_{\max}(t_n) < 1$	$a_{\max}(t_n) < 1$	$a_{\max}(t_n) < 1$
	10^{-6}	$a_{\max}(t_n) < 1$	$a_{\max}(t_n) < 1$	$a_{\max}(t_n) < 1$	$a_{\max}(t_n) < 1$	$a_{\max}(t_n) < 1$	$a_{\max}(t_n) < 1$
5	10^{-1}	−6.0707	142.2670	−4.4917	1.2517	−2.6669	1.0111
	10^{-2}	−6.4740	143.3143	−0.8229	1.1113	−4.5594	1.0759
	10^{-4}	$a_{\max}(t_n) < 1$	$a_{\max}(t_n) < 1$	$a_{\max}(t_n) < 1$	$a_{\max}(t_n) < 1$	$a_{\max}(t_n) < 1$	$a_{\max}(t_n) < 1$
	10^{-6}	$a_{\max}(t_n) < 1$	$a_{\max}(t_n) < 1$	$a_{\max}(t_n) < 1$	$a_{\max}(t_n) < 1$	$a_{\max}(t_n) < 1$	$a_{\max}(t_n) < 1$
10	10^{-1}	−5.6307	508.5643	−4.5248	1.4802	−3.6825	1.4577
	10^{-2}	−4.7718	508.1754	−3.2235	1.7201	−4.5594	1.5638
	10^{-4}	−6.4808	511.1265	−4.5255	1.5332	−4.1548	1.7381
	10^{-6}	$a_{\max}(t_n) < 1$	$a_{\max}(t_n) < 1$	−4.5255	1.6749	−4.5594	1.8848
15	10^{-1}	−6.4806	1138.4	−4.5255	1.9245	−4.3178	1.9437
	10^{-2}	−6.4804	1150.2	−4.5255	1.9017	−4.4443	1.9593
	10^{-4}	−6.4807	1146.01	−3.1743	1.9600	−4.5594	2.0781
	10^{-6}	−6.4808	1144.3	−4.5254	1.8854	−4.4564	2.0389

time than that of the HOHC-FEM algorithm. Hence, the algorithm HOHC-RPIM seems to be a competitive approach to solve nonlinear problems.

To investigate the temporal evolution of temperature, we choose the point $P1$ located at $x = 0.5$ and $y = 0.5$ represented in Figure 2. The temporal evolution of temperature at this point obtained by three algorithms is shown in Figure 3. This comparison of temperature evolution regards the results obtained by HOHC-RPIM, NR-RPIM, and NR-FEM algorithms in cases of linear and nonlinear heat conduction. From this figure, it can be seen that the obtained results coincide well with those calculated by the NR-RPIM and the NR-FEM. This shows the correctness and the ability of the proposed approach. It can also be seen that the evolution of temperature in the linear case where $e = 0$ does not even reach the steady state in the interval time $[0, 100s]$ contrary to the nonlinear effects.

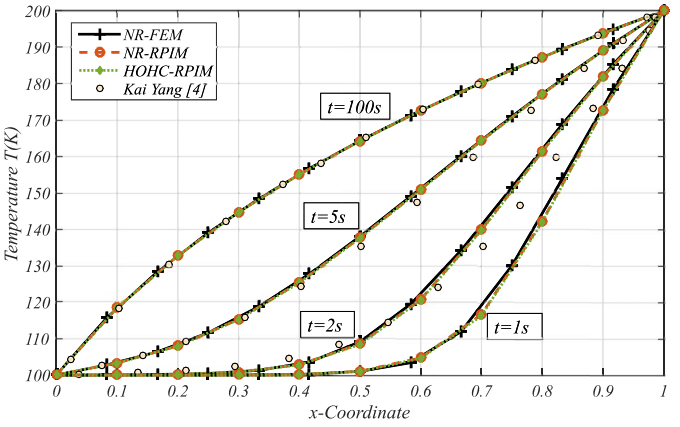

Figure 4. Temperature distribution along the line $y = 0.5$ at times $t = 1,2,5$, and 100 s obtained by the three algorithms.

Figure 4 shows the temperature distribution along the line $y = 0.5$ at times $t = 1,2,5$, and 100 s. The comparison among the obtained results shows that they are in good agreement.

In Figure 5, we illustrate the isothermal solutions at $t = 1,5$, and 100 s obtained by the HOHC-RPIM and NR-FEM algorithms. These solutions are identical and similar to those presented in the literature [4] with CPU times 0.7619 s for the HOHC-RPIM and 220.083 s for the NR-FEM. It is noted that the heat flux and the temperature gradient dynamically change when the temperature increases with time. Solving this problem needs two inversions of the pre-conditioner $[K^*]$ by the proposed approach HOHC-RPIM with $P = 3$ and $\kappa = 10^{-1}$. However, by the NR-RPIM and NR-FEM algorithms, this resolution requires 1428 and 1299 inversions of the tangent matrix respectively with tolerance $\varepsilon = 10^{-6}$.

5.2. *Heat conduction over a perforated circular plate with a circular hole*

As the second example, we consider the heat conduction in a perforated circular plate of internal and external radii $r_1 = 0.3$ m and $r_2 = 1$ m, respectively [41] (see Figure 6). The domain occupied by the plate is replaced by 636 nodes for the HOHC-RPIM algorithm and discretized by 1157 finite elements of type $T3$ for the HOHC-FEM algorithm. The same parameters of the proposed approach in the first example are adopted in this study (i.e., truncation order $P = 3$ and a tolerance parameter $\kappa = 10^{-1}$). The boundary and initial conditions associated with this problem are given as follows:

$$\text{Case 1}\begin{cases} T(X,t) = 200\ \text{K} & \text{at } x^2+y^2 = r_1^2 \qquad \forall\, t \\ T(X,t) = 100\ \text{K} & \text{at } x^2+y^2 = r_2^2 \qquad \forall\, t \\ T(X,t) = 100\ \text{K} & \text{at } r_1^2 < x^2+y^2 < r_2^2 \quad t = 0 \end{cases}$$
$$\text{Case 2}\begin{cases} T(X,t) = 200\ \text{K} & \text{at } x^2+y^2 = r_1^2 \qquad \forall\, t \\ -k(T)\dfrac{\partial T}{\partial N} = 0 & \text{at } x^2+y^2 = r_2^2 \qquad \forall\, t \\ T(X,t) = 100\ \text{K} & \text{at } r_1^2 < x^2+y^2 < r_2^2 \quad t = 0. \end{cases} \tag{15}$$

The temperature evolution with respect to time at the node located at $(x = r_2 + r_1/2, y = 0)$ is presented in Figure 7 for both cases of boundary conditions, which are defined by (15). This figure

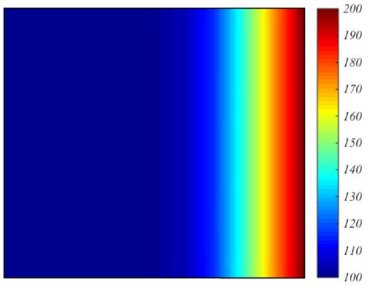

(a) Isothermal distribution at $t = 1s$ using HOHC-RPIM

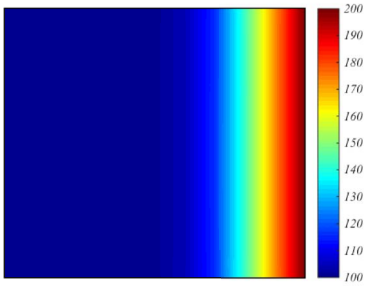

(b) Isothermal distribution at $t = 1s$ using NR-FEM

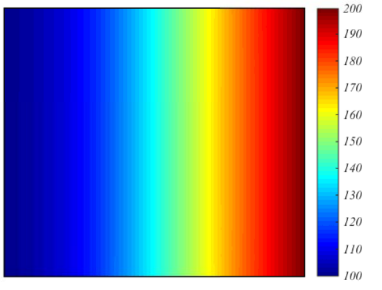

(c) Isothermal distribution at $t = 5s$ using HOHC-RPIM

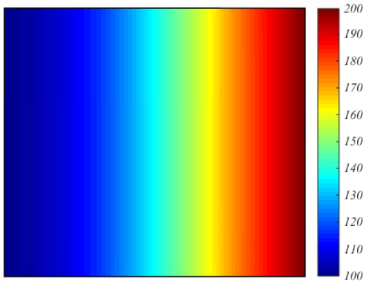

(d) Isothermal distribution at $t = 5s$ using NR-FEM

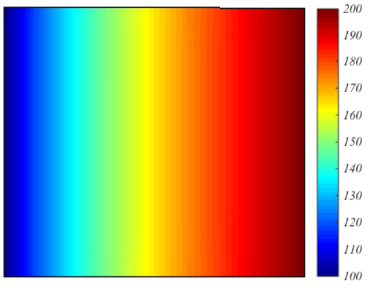

(e) Isothermal distribution at $t = 100s$ using HOHC-RPIM

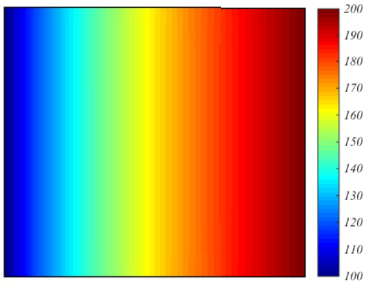

(f) Isothermal distribution at $t = 100s$ using NR-FEM

Figure 5. Isothermal distribution in the plate: comparison between HOHC-RPIM and NR-FEM algorithms.

shows a comparison of temperature evolution among the three algorithms HOHC-RPIM, HOHC-MLS, and HOHC-FEM. The obtained results are in good agreement. In addition, the effects of boundary conditions on the temperature can be easily observed.

To investigate the temperature evolution with respect to time and the line $x = 0$ or $y = 0$, we proceed to construct the considered sections of the components of the temperature on the line $y \approx 0$ for $x \in [-r_2, r_2]$ (see Figure 6b). In Figure 8, we represent the temperature evolution along the line x for $y \approx 0$ for times $t = 0.1, 1, 3, 5, 10$, and 15 s for cases 1 and 2. In this example, we observe that in case 1, at the steady state, the temperature reaches an average of both temperatures

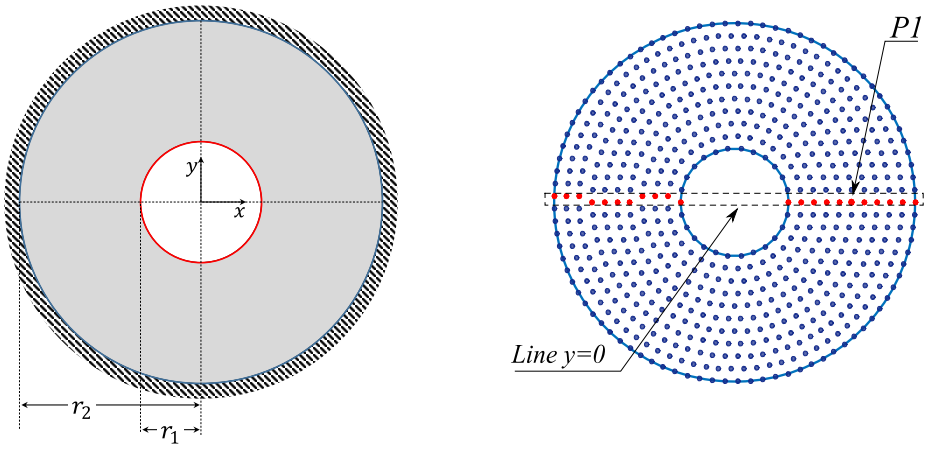

(a) Continuous domain (b) Discrete domain

Figure 6. Continuous and discrete domains.

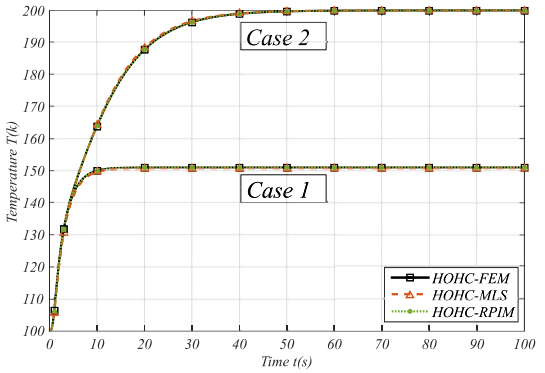

Figure 7. Temporal evolution of temperature at the node of coordinate $(x = r_2 + r_1/2, y = 0)$.

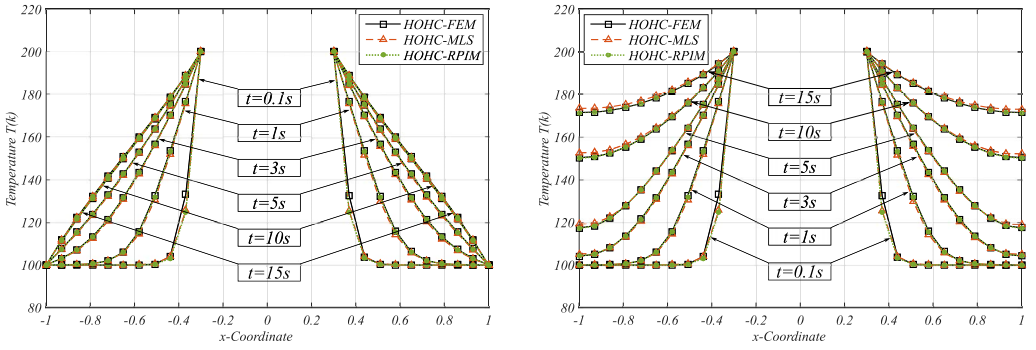

(a) Case 1 (b) Case 2

Figure 8. Temperature evolution along the line x for $y \approx 0$ obtained by the three algorithms.

imposed at inner and outer boundaries. However, the insulated boundary in case 2 indicates that the temperature of the plate increases without exceeding the temperature imposed on the inner

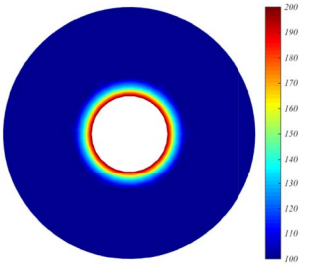

(a) Isothermal distribution at $t = 0.1s$: case 1

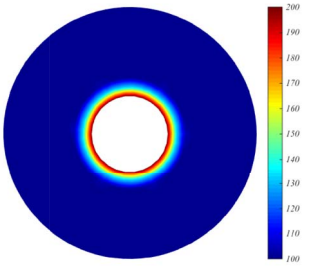

(b) Isothermal distribution at $t = 0.1s$: case 2

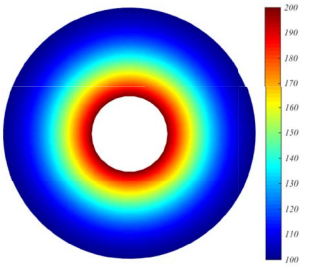

(c) Isothermal distribution at $t = 3s$: case 1

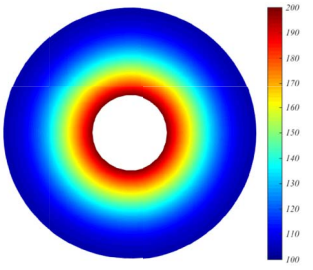

(d) Isothermal distribution at $t = 3s$: case 2

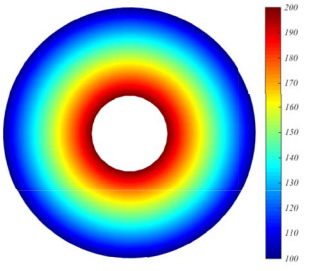

(e) Isothermal distribution at $t = 10s$: case 1

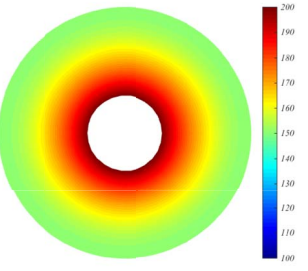

(f) Isothermal distribution at $t = 10s$: case 2

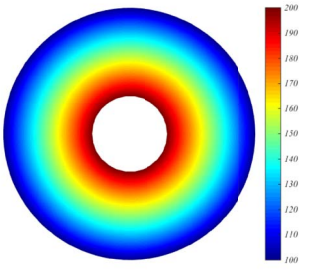

(g) Isothermal distribution at $t = 15s$: case 1

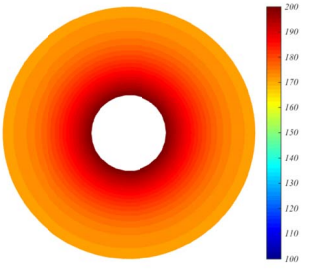

(h) Isothermal distribution at $t = 15s$: case 2

Figure 9. Isothermal distribution: comparison between both cases at different moments.

boundary due to the thermal insulation imposed on the outer boundary.

In Figure 9, we illustrate the comparison of the isothermal distributions between both cases at different moments $t = 0.1, 3, 10$, and 15 s. This figure follows the same remarks from previous statements.

6. Conclusion

In this paper, the RPIM is implemented in high-order homotopic continuation to solve nonlinear transient inverse heat conduction problems. The introduction of the homotopy technique makes it possible to reduce computation time in terms of tangent matrix inversions. The proposed approach is used for identifying temperature-dependent thermal conductivity. The obtained results are compared with those calculated by the solvers NR-RPIM, NR-FEM, HOHC-FEM, and HOHC-MLS. This comparison has demonstrated the correctness and the reliability of the proposed approaches NR-RPIM and HOHC-RPIM. This is a competitive approach that is an alternative solver for nonlinear heat conduction problems with any kind of temperature-dependent conductivity.

References

[1] A. Khosravifard, M. R. Hematiyan, L. Marin, "Nonlinear transient heat conduction analysis of functionally graded materials in the presence of heat sources using an improved meshless radial point interpolation method", *Appl. Math. Modelling* **35** (2011), no. 9, p. 4157-4174.

[2] X. Zhang, H. Xiang, "A fast meshless method based on proper orthogonal decomposition for the transient heat conduction problems", *Int. J. Heat Mass Transfer* **84** (2015), p. 729-739.

[3] M. Dehghan, M. S. Valipour, S. Saedodin, "Temperature-dependent conductivity in forced convection of heat exchangers filled with porous media: a perturbation solution", *Energy Convers. Manage.* **91** (2015), p. 259-266.

[4] K. Yang, H. F. Peng, J. Wang, C. H. Xing, X. W. Gao, "Radial integration BEM for solving transient nonlinear heat conduction with temperature-dependent conductivity", *Int. J. Heat Mass Transfer* **108** (2017), p. 1551-1559.

[5] K. Yang, W. Z. Feng, J. Wang, X. W. Gao, "RIBEM for 2D and 3D nonlinear heat conduction with temperature dependent conductivity", *Eng. Anal. Bound. Elem.* **87** (2018), p. 1-8.

[6] J. Y. Chang, C. C. Tsai, D. L. Young, "Homotopy method of fundamental solutions for solving nonlinear heat conduction problems", *Eng. Anal. Bound. Elem.* **108** (2019), p. 179-191.

[7] J. C. Álvarez Hostos, A. D. Bencomo, E. S. Puchi-Cabrera, V. D. Fachinotti, B. Tourn, J. C. Salazar-Bove, "Implementation of a standard stream-upwind stabilization scheme in the element-free Galerkin based solution of advection-dominated heat transfer problems during solidification in direct chill casting processes", *Eng. Anal. Bound. Elem.* **106** (2019), p. 170-181.

[8] P. R. Lancaster, K. Salkauskas, "Surfaces generated by moving least squares methods", *Math. Comput.* **155** (1981), p. 141-158.

[9] G. R. Liu, Y. T. Gu, "A point interpolation method for two-dimensional solids", *Int. J. Numer. Methods Eng.* **50** (2001), no. 4, p. 937-951.

[10] J. G. Wang, G. R. Liu, "A point interpolation meshless method based on radial basis functions", *Int. J. Numer. Methods Eng.* **54** (2002), no. 11, p. 1623-1648.

[11] G. R. Liu, Y. T. Gu, *An Introduction to Meshfree Methods and their Programming*, Springer Science & Business Media, 2005.

[12] V. P. Nguyen, T. Rabczuk, S. Bordas, M. Duflot, "Meshless methods: a review and computer implementation aspects", *Math. Comput. Simul.* **79** (2008), no. 3, p. 763-813.

[13] M. Najafi, V. Enjilela, "Natural convection heat transfer at high Rayleigh numbers-extended meshless local Petrov-Galerkin (MLPG) primitive variable method", *Eng. Anal. Bound. Elem.* **44** (2014), p. 170-184.

[14] R. Wang, L. Zhang, D. Hu, C. Liu, X. Shen, C. Cho, B. Li, "A novel approach to impose periodic boundary condition on braided composite RVE model based on RPIM", *Compos. Struct.* **163** (2017), p. 77-88.

[15] X. Y. Cui, S. Z. Feng, G. Y. Li, "A Cell-based Smoothed Radial Point Interpolation Method (CS-RPIM) for heat transfer analysis", *Eng. Anal. Bound. Elem.* **40** (2014), p. 147-153.

[16] O. Bourihane, B. Braikat, M. Jamal, F. Mohri, N. Damil, "Dynamic analysis of a thin-walled beam with open cross section subjected to dynamic loads using a high-order implicit algorithm", *Eng. Struct.* **120** (2016), p. 133-146.

[17] F. Massa, I. Turpin, T. Tison, "From homotopy perturbation technique to reduced order model for multiparametric modal analysis of large finite element models", *Mech. Syst. Signal Process.* **96** (2017), p. 291-302.

[18] Y. Guevel, G. Girault, J. M. Cadou, "Numerical comparisons of high-order nonlinear solvers for the transient navier-stokes equations based on homotopy and perturbation techniques", *J. Comput. Appl. Math.* **289** (2015), p. 356-370.
[19] B. Claude, L. Duigou, G. Girault, J. M. Cadou, "Study of damped vibrations of a vibroacoustic interior problem with viscoelastic sandwich structure using a High Order Newton solver", *J. Sound Vib.* **462** (2019), article no. 114947.
[20] A. Timesli, B. Braikat, H. Lahmam, H. Zahrouni, "An implicit algorithm based on continuous moving least square to simulate material mixing in friction stir welding process", *Modelling Simul. Eng.* **2013** (2013), p. 1-14.
[21] A. Timesli, B. Braikat, H. Lahmam, H. Zahrouni, "A new algorithm based on moving least square method to simulate material mixing in friction stir welding", *Eng. Anal. Bound. Elem.* **50** (2015), p. 372-380.
[22] Y. Belaasilia, A. Timesli, B. Braikat, M. Jamal, "A numerical mesh-free model for elasto-plastic contact problems", *Eng. Anal. Bound. Elem.* **82** (2017), p. 68-78.
[23] S. Mesmoudi, A. Timesli, B. Braikat, H. Lahmam, H. Zahrouni, "A 2D mechanical-thermal coupled model to simulate material mixing observed in friction stir welding process", *Eng. Comput.* **33** (2017), no. 4, p. 885-895.
[24] Y. Belaasilia, B. Braikat, M. Jamal, "High order mesh-free method for frictional contact", *Eng. Anal. Bound. Elem.* **94** (2018), p. 103-112.
[25] M. Fouaidi, A. Hamdaoui, M. Jamal, B. Braikat, "A high order mesh-free method for buckling and post-buckling analysis of shells", *Eng. Anal. Bound. Elem.* **99** (2019), p. 89-99.
[26] M. Rammane, S. Mesmoudi, A. Tri, B. Braikat, N. Damil, "Solving the incompressible fluid flows by a high-order mesh-free approach", *Int. J. Numer. Methods Fluids* **92** (2020), no. 5, p. 422-435.
[27] S. Mesmoudi, B. Braikat, H. Lahmam, H. Zahrouni, "Three-dimensional numerical simulation of material mixing observed in FSW using a mesh-free approach", *Eng. Comput.* **36** (2020), p. 13-27.
[28] M. Fouaidi, A. Hamdaoui, M. Jamal, B. Braikat, "Numerical analysis of single-layered graphene sheets by a mesh-free approach", *Eng. Comput.* (2020), p. 1-14, in press.
[29] O. Askour, S. Mesmoudi, B. Braikat, "On the use of Radial Point Interpolation Method (RPIM) in a high order continuation for the resolution of the geometrically nonlinear elasticity problems", *Eng. Anal. Bound. Elem.* **110** (2020), p. 69-79.
[30] B. Yun, W. T. Ang, "A dual-reciprocity boundary element approach for axisymmetric nonlinear time-dependent heat conduction in a nonhomogeneous solid", *Eng. Anal. Bound. Elem.* **34** (2010), no. 8, p. 697-706.
[31] P. W. Li, W. Chen, Z. J. Fu, C. M. Fan, "Generalized finite difference method for solving the double-diffusive natural convection in fluid-saturated porous media", *Eng. Anal. Bound. Elem.* **95** (2018), p. 175-186.
[32] M. Mierzwiczak, J. A. Kołodziej, "The determination temperature-dependent thermal conductivity as inverse steady heat conduction problem", *Int. J. Heat Mass Transfer* **54** (2011), no. 4, p. 790-796.
[33] M. Mierzwiczak, W. Chen, Z. J. Fu, "The singular boundary method for steady-state nonlinear heat conduction problem with temperature-dependent thermal conductivity", *Int. J. Heat Mass Transfer* **91** (2015), p. 205-217.
[34] K. Yang, G. H. Jiang, H. F. Peng, X. W. Gao, "A new modified Levenberg–Marquardt algorithm for identifying the temperature-dependent conductivity of solids based on the radial integration boundary element method", *Int. J. Heat Mass Transfer* **144** (2019), article no. 118615.
[35] M. I. P. Hidayat, "Meshless local B-spline collocation method for heterogeneous heat conduction problems", *Eng. Anal. Bound. Elem.* **101** (2019), p. 76-88.
[36] J. Singh, K. K. Shukla, "Nonlinear flexural analysis of laminated composite plates using RBF based meshless method", *Compos. Struct.* **94** (2012), no. 5, p. 1714-1720.
[37] J. Singh, K. K. Shukla, "Nonlinear flexural analysis of functionally graded plates under different loadings using RBF based meshless method", *Eng. Anal. Bound. Elem.* **36** (2012), no. 12, p. 1819-1827.
[38] J. Li, X. Feng, Y. He, "RBF-based meshless Local Petrov Galerkin Method for the multi-dimensional convection–diffusion-reaction equation", *Eng. Anal. Bound. Elem.* **98** (2019), p. 46-53.
[39] B. Cochelin, "A path-following technique via an asymptotic-numerical method", *Comput. Struct.* **53** (1994), p. 1181-1192.
[40] K. Yang, J. Wang, J. M. Du, H. F. Peng, X. W. Gao, "Radial integration boundary element method for nonlinear heat conduction problems with temperature-dependent conductivity", *Int. J. Heat Mass Transfer* **104** (2017), p. 1145-1151.
[41] Y. Gu, L. Wang, W. Chen, C. Zhang, X. He, "Application of the meshless generalized finite difference method to inverse heat source problems", *Int. J. Heat Mass Transfer* **108** (2017), p. 721-729.